# COMPUTATION OF TURBULENT FLOW AND HEAT TRANSFER OVER A WAVY WALL CHANNEL EMPLOYING AN EXPLICIT ALGEBRAIC STRESS MODEL

A. Azzi[1], A. Z. Dellil[2] and B. A. Jubran[3]

1. Faculté de Génie-Mécanique, Université des Sciences et de la Technologie d'Oran, Algérie.
Email : azzi@algeriecom.com
2. Faculté des sciences, Université d'Oran Es-sénia, Algérie.
3. Sultan Qaboos University, Department of Mechanical and Industrial Engineering,
Muscat, Sultanate of Oman

## ABSTRACT

This paper presents some recent trends in modeling of anisotropic turbulent near wall flow and heat transfer. The aim is to test the predictive performance of explicit algebraic stress models to reproduce the near wall flow and heat transfer over a wavy wall. The study focus on explicit algebraic stress models, up to cubic fragments of strain and vorticity tensors and rigorously derived from second-moment closure. The stress-strain relations are resolved in the context of a two-layer strategy resolving the near wall region by means of a non-linear one equation model and the outer core flow is treated by use of the two-equations model.
In a first step, selected models were employed for calculating the fully turbulent channel flow, which is documented by large DNS database. Comparison of Reynolds Stress tensor components shows a perfect ability of the models to reproduce reasonably the trend of the flow. The models are then extended to calculate the flow over a wavy wall. Comparisons of the present computations, previous calculations with isotropic eddy viscosity model and DNS data show that the present models are successful in capturing the anisotropic feature of the flow. However, only the trend of variation of the stress tensor components can be reproduced by the models. The predicted results show also, the shortcomings of the standard law of the wall for predicting such type of flows and consequently suggest that direct integration to the wall must be used instead.

**Keywords :** Wavy wall, heat transfer enhancement, anisotropic turbulence models, finite volume method, wall functions

## NOMENCLATURE

| | |
|---|---|
| $x_i$ | general non-orthogonal coordinate system |
| $J$ | Jacobien of the coordinate transformation |
| $f$ | time averaged variable |
| $C_i$ | convection term |
| $D_i^f$ | diffusion term |
| $S_f$ | source term |
| $d_{ij}$ | Kronecker delta |
| $\overline{u_i u_j}$ | Reynolds stress tensor |
| $\overline{u_j q}$ | turbulent heat flux |
| $k$ | turbulent kinetic energy |
| $\Gamma_{ij}$ | turbulent transport coefficient |
| $\mathrm{Pr}_t$ | turbulent Prandtl number |
| $S_{ij}$ | mean rate of strain |
| $n_t$ | isotropic eddy viscosity |
| $C_m$ | model constant, $=0.082$ |
| $e$ | rate of dissipation of $k$ |
| $l_m$ , $l_e$ | length scales, eqs (7) and (9) |
| $k$ | von Karman constant, $=0,4$ |
| $f_m$ | damping function, eq. (8) |
| $R_y$ | turbulent Reynolds number, eq. (10) |
| $r$ | density |
| $H$ | inter wall spacing |
| $am$ | wave amplitude |
| $l$ | wave length |
| $U_t$ | friction velocity, ( $\sqrt{t_w/r}$ ) |
| Re | Reynolds number, $(HU/n)$ |

## 1. INTRODUCTION

Wavy wall heat transfer enhancement technique has been used extensively in the design of compact heat exchangers as can be seen from the numerous experimental and numerical investigations reported in the literature. Recently, Hudson et al. [1] studied experimentally a rectangular water channel where the lower wall was constructed with removable Plexiglas plates on which the waves were milled. To insure that a fully periodic flow had developed, the LDV measurements were made above the 31st of 36 waves. The wavelength and the amplitude were set to $(l = H)$ and $(am = 0.05H)$, respectively, where $H$ is the mean height of the channel. This experimental work is one of the few studies which provides extensive measurements of the Reynolds stresses. The study was followed by Direct Numerical Simulation reported by Maaß and Schumann [2], and hence it was selected as a benchmark to validate the dynamic part of the present computation. This type of turbulent flow is numerically very challenging, since it is characterized by periodic changes of the pressure gradient, curved streamlines, and for important wave amplitude, separation and reattachment can occur. So, it is expected that isotropic eddy viscosity turbulence models can not reproduce perfectly the turbulent quantities of such flow. The goal of the present study is to test the ability of selected explicit algebraic stress models to reproduce the right trend of near wall flow and heat transfer. The wall boundary conditions were applied by using a new zonal modeling strategy based on DNS data and combining the EASM turbulence model in the outer core flow and a one equation model resolving the near-wall region. This strategy was initialized by Rodi et al. [3] and tested with success in previous computations [4].

## 2. THE MATHEMATICAL MODEL

The mathematical model consists of the RANS, the two-equation eddy viscosity k-ε turbulence model and the energy equation. The governing equations for steady, turbulent, incompressible flows in non-orthogonal co-ordinates using Cartesian velocity components can be written in a generalized form as follows:

$$\frac{1}{J}\frac{\P}{\P x_i}\left(C_i f + D_i^f\right) = S_f \,, \qquad (1)$$

Where $f$ is the considered time-averaged variable, $J$ is the Jacobian of the coordinate transformation, $C_i$, $D_i^f$ represent respectively the convection and the diffusion terms and $S_f$ is the source term. The above terms for each considered dependent variable are explicitly indicated in the previous paper [4].

A first computation was done where the Reynolds-stress tensor and the turbulent heat flux are approximated within the context of the k-ε turbulence model and the near-wall viscosity-affected region is resolved with a one-equation model [3]. The two-layer approach represents an intermediate modeling strategy between wall function and pure low-Reynolds number model. It consists of resolving the viscosity-affected regions close to the wall with a one-equation model. In the outer core flow, the usual eddy-viscosity hypothesis is used, applying a linear relation of the Reynold-stress tensor to the velocity gradient as follows:

$$\overline{u_i' u_j'} = \frac{2}{3}d_{ij}k - 2\Gamma_{ij}S_{ij} \qquad (2)$$

$$\overline{u_j q} = -\frac{\Gamma_{ij}}{\mathrm{Pr}_t}\frac{\partial \overline{T}}{\partial x_j} \qquad (3)$$

where $d_{ij}$ is the Kronecker delta, $k \equiv \overline{u_i' u_j'}/2$ is the turbulent kinetic energy, and $S_{ij}$ is the rate of strain tensor. For high-Re flows, the turbulent transport coefficient $\Gamma_{ij}$ is conventionally made isotropic and proportional to a velocity scale $(\sim k)$ and a time scale $(k/e)$, characterizing the local rate of turbulence and is given by:

$$\Gamma_{ij} \equiv n_t \equiv C_m k^2/e \qquad (4)$$

where $n_t$ is known as the isotropic eddy viscosity, $e$ represents the rate of dissipation of $k$, and $C_m$ stand for a model constant. The distributions of $k$ and $e$ are determined from the conventional model transport equations of Jones and Launder [5], and standard values can be assigned to the model constants. In this flow region the turbulent Prandtl number is usually fixed at 0.9. In the one equation model, the eddy viscosity is made proportional to a velocity scale determined by solving the $k$-equation, and a length scale $l_m$ prescribed

algebraically. The dissipation rate $e$ is related to the same velocity scale and a dissipation length scale $l_e$, also prescribed algebraically [3]. Such model has the advantage of requiring considerably fewer grid points in the viscous sub-layer than any pure Low Reynolds scheme. Also, because of the fixed length-scale distribution near the wall, these models have been found to give better prediction for adverse pressure gradient boundary layer than pure $k-e$ models.

The present two-layer model is a re-formulated version of the so-called $\left(\overline{v'^2}\right)$ velocity-scale based model (TLV) proposed by Rodi et al. [3]. In a recent study Azzi and Lakehal [4] re-incorporate $k^{1/2}$ as a velocity scale instead $\left(\overline{v^2}\right)^{1/2}$ and $l_m$ and $l_e$ are re-scaled on the basis of the same DNS data of Kim et al. [6]. This model will be call hereafter as SKE-TLV model and defined as follows:

$$\Gamma_{ij} \equiv \mu_t \equiv C_m \sqrt{k}\, l_m \tag{5}$$

$$e = k^{3/2} / l_e \tag{6}$$

$$l_m = k\, y\, C_m^{-3/4} f_m \tag{7}$$

$$f_m = \frac{1}{32}\sqrt{0{,}116 \times R_y^2 + R_y} \tag{8}$$

$$l_e = \frac{k\, C_m^{-3/4} y}{2 + 17.29 / \left(f_m R_y k\, C_m^{-3/4}\right)} \tag{9}$$

$$R_y = r\, \sqrt{k}\, y / m \tag{10}$$

Where $k = 0{,}4$ and $C_m = 0{,}082$. The outer and the near-wall model are matched at the location where $f_m = 0.95$, indicating that viscous effects become negligible. More details can be found in [4], where the model is tested for a fully developed channel and applied for a film cooling configuration.

Three Explicit Algebraic Stress Models were selected to be used in comparison with the reference model cited above. The idea of such models is to approximate each of the Reynolds stress components in order to keep the anisotropic features of the Reynolds stress models without solving their transport equations. The common starting point of this type of models is the assumption of homogeneous turbulent flows in the limit of equilibrium, leading to a similar explicit expression for $\overline{u_i' u_j'}$ which, in non-rotating frames takes the following form:

$$\overline{u_i' u_j'} = \frac{2}{3} d_{ij} k - 2\tilde{\mu}_t \left[ S_{ij} + \sum_n C^n T_{ij}^n \right]; \qquad \tilde{\mu}_t = \tilde{C}_m\, k^2 / e \tag{11}$$

where the $T_{ij}^n$ are the products of the strain and vorticity tensors, $S_{ij}$ and $\Omega_{ij}$. The available models differ in the way the coefficients $C^n$ and $\tilde{C}_m$ are determined, and in the number of strain and vorticity-stress products, i.e., quadratic, cubic, etc. Three model variants have been selected in the present study: one of them is quadratic and two are cubic with respect to $S_{ij}$ and $\Omega_{ij}$; namely the quadratic model of Gatski and Speziale [7] (GS), the cubic model of Craft et al. [8] (CL96) and again the cubic model of Lien et al. [9] (LC96). Details of each of these models can be found in the corresponding references.

## 3. NUMERICAL PROCEDURE

The numerical procedure used to calculate the test case is based on a finite-volume approach for implicitly solving the incompressible Reynolds Averaged Navier Stokes equations (RANS) on arbitrary non-orthogonal grids, employing a cell-centred grid arrangement. The momentum-interpolation technique of Rhie and Chow [10] is used to prevent pressure-field oscillations and the pressure-velocity coupling is achieved using the SIMPLEC algorithm of Van Doormal and Raithby [11]. The resulting system of the algebraic difference equations is solved using the Strongly Implicit Procedure (SIP) of Stone [12]. The convection fluxes are approximated by employing the QUICK scheme for all variables applied in a scalar form by means of a deferred-correction procedure and bounded by the Van-Leer Harmonic function as limiter. The diffusive fluxes are, however, approximated using second-order central differences. More details of the mathematical

formulation, which are now a standard material and well known to most investigators, can be found in the following references [13-14].

## 4. COMPUTATIONAL DOMAIN AND BOUNDARY CONDITIONS

Figure 1 shows the computational domain and the boundary conditions. The wavy and the flat plate are placed with a mean spacing $(H=1)$. The amplitude and the wavelength of the lower sinusoidal wavy wall are $(am=0.05H)$ and $(l=H)$, respectively. The upstream and downstream flat sections ($4l$ and $2l$ in length) are used for flow adjustment and flow recovery, respectively. This technique was used previously with success by Patel et al. [2]. The first run was done for a *80H* straight channel and a fully developed flow distribution at the exit which was subsequently used as the inlet flow boundary conditions for the next computations. The Reynolds number was set as in DNS computations [2] at $\mathrm{Re}(HU/n)=6760$. The turbulence intensity is assigned a value of *5%* and the turbulence dissipation is calculated based on a turbulent viscosity equal *50* times the laminar viscosity. At the outflow boundary, zero-gradient conditions are imposed for all dependent variables.

## 5. GRID MESH

The quality of a computational solution is strongly linked to the quality of the grid mesh. So a highly orthogonalized, nonuniform, fine grid mesh was generated with grid nodes considerably refined in the near-wall region. The normalized $y^+$ values at the near wall node are less than unity, and care is taken so that the stretching factors are kept close to unity. Figure 2 shows a close-up of the computational grid used for the case with $am=0.10H$. The grid adopted for the computations was obtained after a series of tests and consists of *42,100* grid nodes (disposed on a global array $421\times100$ nodes in *x,* and *y* directions).

## 6. RESULTS AND DISCUSSION

Figures 3, 4, 5 and 6 compare the normalized mean velocity, turbulent kinetic energy, normal stress component and shear stress profiles with DNS data. The comparison is done until the middle of the channel and at four streamwise locations of the seventh wave that correspond to the divergent, trough, convergent and crest positions respectively (x/H= *0.3, 0.5, 0.8* and *1.0*). The first panel of each figures show reasonable agreement for the mean velocity profiles. The reverse flow occurring in the first half of the wave (*x/H= 0.3 and 0.5*) is clearly captured by all models. The present computation confirm what is expected that most turbulence models are able to reproduce reasonably the velocity profiles. However, the turbulent kinetic energy presented in the second panel is globally underpredicted at all stations and by all models. As it was observed in an earlier test on flow over flat plate [4], this underprediction is a consequence of an overpredicted value of the turbulence dissipation in the region where $k^+$ reaches its peak value. However, the underprediction is more consistent in this wavy wall case. It can also be observed that turbulent kinetic energy is represented by very different plots along the streamwise direction of the wave and until approximately *0.25H* normal to the wall. The maximum peak is observed at *x/H=0.5* in the streamwise direction and roughly at *0.05H* normal to the wall. We note also, that all models reproduce perfectly the trend of lateral variation of $k^+$ at all stations.

Panel ( c ) of the figures represent the streamwise normal stress component compared with DNS data. Here, the difference between the models is clearly perceptible. One can see that the ske-TLV model is unable to reproduce the right trend of the $u'u'$ profile. At divergent and convergent stations which correspond at *x/H= 0.3 and 0.8* respectively (figures 3c and 5c) the GS-LT and CL96 are both able to reproduce the trend of DNS data while in the other two stations the prediction is poor, specially at figure 6c where occur the first peak near the wall.

The last panel reproduce the shear stress compared to DNS data. Except at divergent station (*x/H= 0.3*) only the trend is reproduced by all models.

Figure 7 shows the normalized logarithmic axial velocity and temperature profiles at trough and crest of the seventh wave computed with the ske-TLV model. In the figure, $U^+$ and $y^+$ are computed with the friction velocity $U_t$ based on the local wall shear stress. The standard velocity and temperature logarithmic laws are also plotted in the figure. For comparison, the computed profiles for the flat plate and for the trough and crest of wavy wall *(0.05H)* are presented. The most important observation is that a standard law is clearly not applicable in such complicated configuration. The strong adverse and favorable pressure gradients are responsible for the new trend shown by the plots. At the crest station, which corresponds to mildly favorable pressure gradient, the velocity and temperature distributions are underpredicted compared with the logarithmic law. At the second

station, which corresponds to the trough, the strong adverse pressure gradient is responsible for the overprediction of the velocity profile compared with that of the logarithmic law. Between the two stations, it can be seen and as expected that there is a zone where the profiles agree with the logarithmic law due to the near zero pressure gradient.
The velocity vector field and the temperature contours are presented in figures 8 and 9. Having in mind that zero value is assigned to the wall and unity value for the inflow, one can see that reattachment points are always recognized by high temperature gradient. We can also see that temperature contours, which are straight in the flat-plate channel, are distorted in the recirculation region when increasing the amplitude waves. This supports the fact that the boundary layer is perturbed by eddies as it is confirmed by the variation of the local Nusselt number through one wave in the fully developed region (figure not presented here). The minimum and the maximum Nusselt numbers are located near the separation and the reattachment points, respectively.

## 7. CONCLUSIONS

Numerical results for the turbulent flow and heat transfer in a two-dimensional channel with wavy wall are presented. The wavy channel studied corresponds to the geometry of Maaß & Schumann [6]. Special attention has been focused on periodic, fully developed thermal and flow fields. Computations have been performed by a finite volume method, solving flow and energy equations. The near-wall viscosity-affected region is resolved with a one-equation model while the outer core of the flow is resolved with standard $k-e$ model as while as with three selected explicit algebraic stress models. The two-layer model is found to be successful in capturing most of the important physical features of such a flow with reasonable amount of memory storage and computer time. The predicted results are globally in good agreement with published DNS data and the EASM models are successful in capturing the anisotropic features of the flow. However, only the trend of variation of the stress tensor components can be reproduced by the models and no clear pictures can be drawn from the present test. The predicted results show also the shortcomings of the standard law of the wall for predicting this type of flows and consequently suggest that direct integrations to the wall must be used instead.

## REFERENCES


1. Hudson J. D., Dykhno L. and Nanratty T. J., Turbulent Production in Flow over a Wavy Wall, Experiments in Fluids, 20, pp. 27-265, 1996.
2. Maaß C. and Schumann U., Direct Numerical Simulation of Separated Turbulent Flow over a Wavy Boundary, in 'Flow Simulation with high performance computers' (ed. Hirschel, E. H.) Notes on Numerical Fluid Mechanics, 52, pp. 227-241, 1996.
3. Rodi, W., Mansour, N. N., and Michelassi, V., 1993, One Equation Near-Wall Turbulence Modelling with the Aide of Direct Simulation Data, Journal of Fluids Engineering, 115, pp. 196-205.
4. Azzi A., and Lakehal D., 2002, Perspectives in Modelling Film-Cooling of Turbine Blades by Transcending Conventional Two-Equation Turbulence Models, ASME, J. of Turbomachinery, Vol. 124, pp. 472-484.
5. Jones W. P. & Launder B. E. Prediction of Relaminarisation with a Two-equation Turbulence Model, Int. Journal of Heat and Mass Transfer, 15, pp. 31-314, 1972.
6. Kim, J., Moin, P., and Moser, R., 1987, Turbulence Statistic in Fully Developed Channel Flow at Low Reynolds Number, Journal of Fluid Mechanics, 177, pp. 133-166.
7. Gatski, T., B., and Speziale, C., G. (1993) "*On Explicit Algebraic Stress Models for Complex Turbulent Flows*," J. Fluid Mech., pp.254, 59-78.
8. Craft, T., J., Launder, B., E., and Suga, K (1996) "*Development and Application of a Cubic Eddy-Viscosity Model of Turbulence,*" Int. J. Heat and Fluif Flow, Vol. 17, N°2, pp.108-115.
9. Lien, F., S., Chen, W., L., and Leschziner, M. (1996) "A., *Low-Reynolds-Nimber Eddy-Viscosity Modelling Based on Non-Linear Stress-Strain/Vorticity Relations,*" Engineering Turbulence Modeling and Experiments 3, W. Rodi and G. Bergeles (Editors), Elsevier Science B. V.
10. Rhie C. M. and Chow W. L., A Numerical Study of the Turbulent Flow Past an Isolated Airfoil with Trailing Edge Separation, AIAA-J., 21, pp. 1225-1532, 1983.
11. Van Doormal J. P. and Raithby G. D., Upstream to Elliptic Problems Involving Fluid Flow, Computers and Fluids, 2, pp. 191-220, 1984.
12. Stone H. L., Iterative Solution of Implicit Approximation of Multidimensional Partial Differential Equations, SIAM J. on Num. Analysis, vol. 5, p.53, 1968.
13. Majumdar S., Rodi W., and Zhu J., Three-Dimensional Finite-Volume Method for Incompressible Flows With Complex Boundaries, Journal of Fluids Engineering, Vol. 114, pp. 496-503, 1992.
14. Zhu, J., An Introduction and Guide to the Computer Program FAST3D, Report No. 691, Institute for Hydromechanics, University of Karlsruhe, 1992.

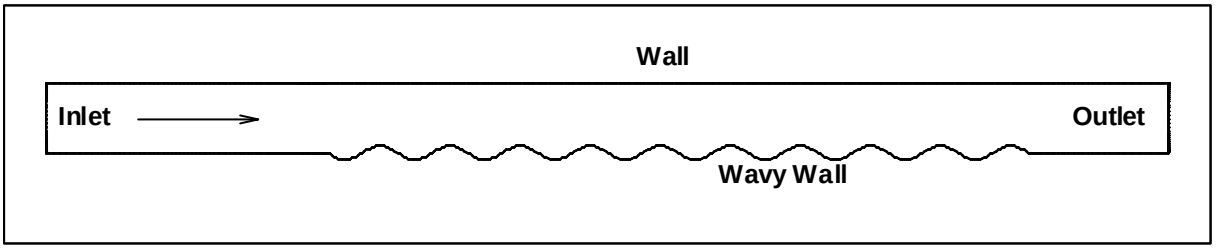


Figure 1 : Geometry and Boundary conditions of the computed wavy wall channel

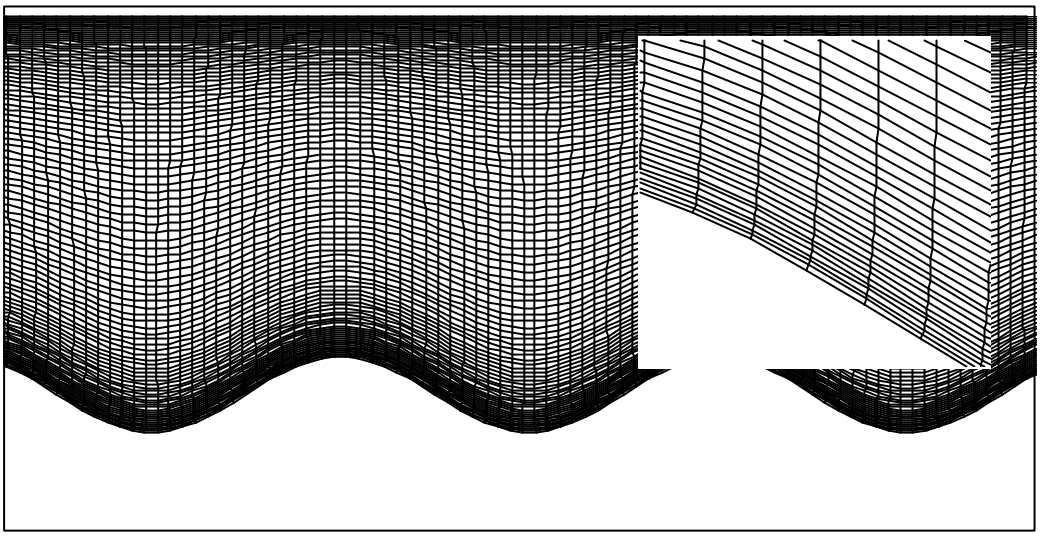

Figure 2: Close-up of the computational grid for the case with 0.1H of amplitude

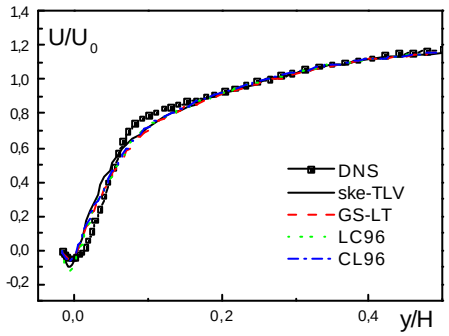


(a) Normalized streamwise mean velocity

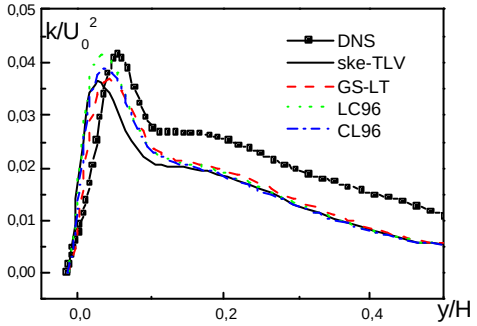


(b) Normalized turbulent kinetic energy

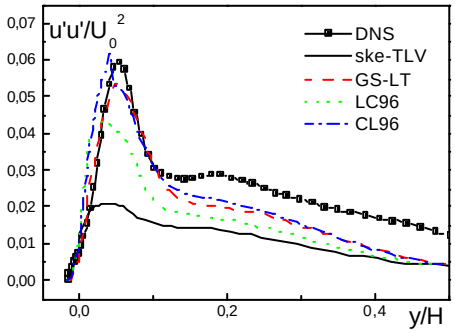


( c ) Normalized turbulent intensity

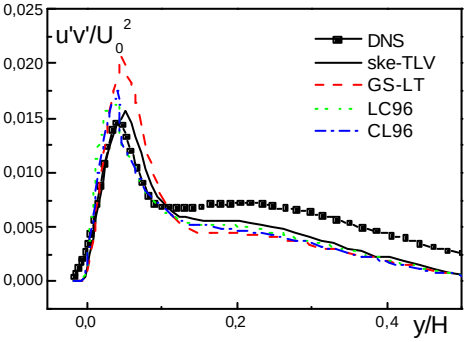


(d) Normalized Reynolds shear stress

Figure 3: Comparison with Maas & Schumann's [2] DNS computation at x/H=0.3.

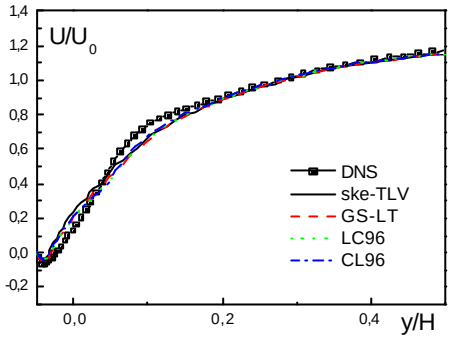


(a) Normalized streamwise mean velocity

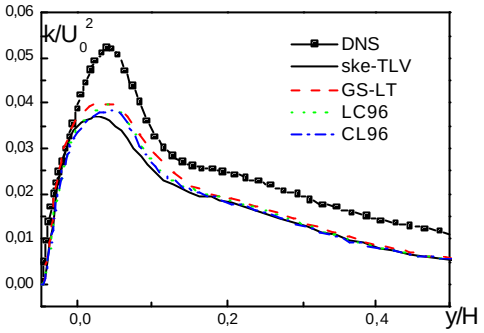


(b) Normalized turbulent kinetic energy

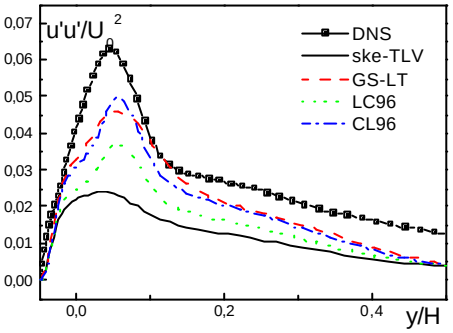


( c ) Normalized turbulent intensity

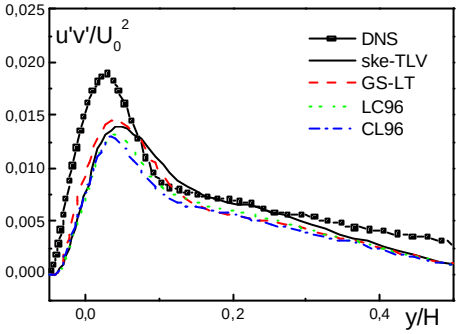


(d) Normalized Reynolds shear stress

Figure 4: Comparison with Maas & Schumann's [2] DNS computation at x/H=0.5.

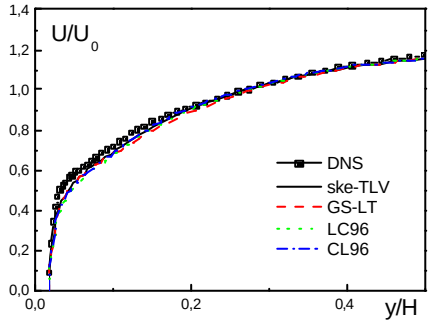


(a) Normalized streamwise mean velocity

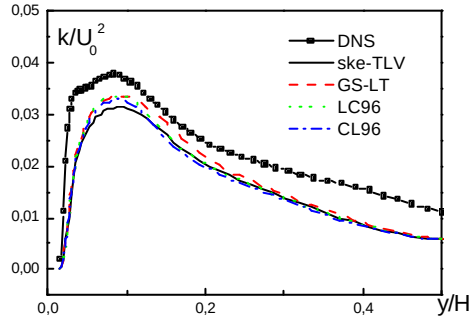


(b) Normalized turbulent kinetic energy

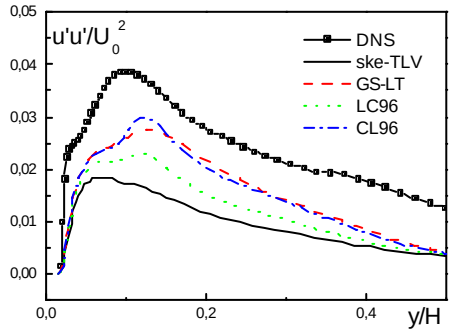


( c ) Normalized turbulent intensity

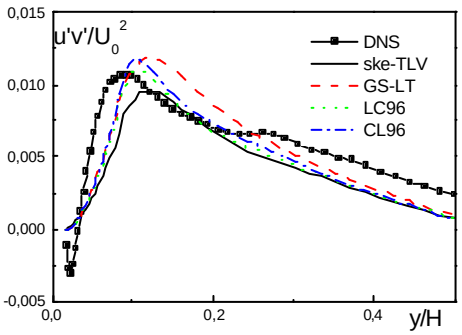


(d) Normalized Reynolds shear stress

Figure 5: Comparison with Maas & Schumann's [2] DNS computation at x/H=0.8.

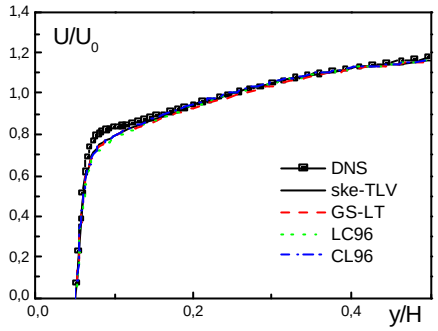


(a) Normalized streamwise mean velocity

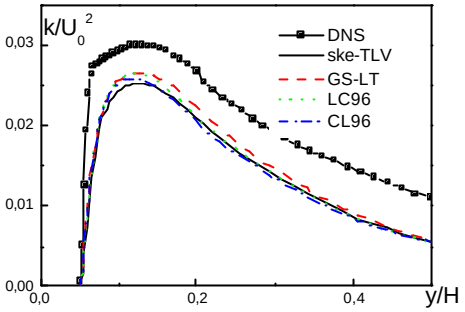


(b) Normalized turbulent kinetic energy

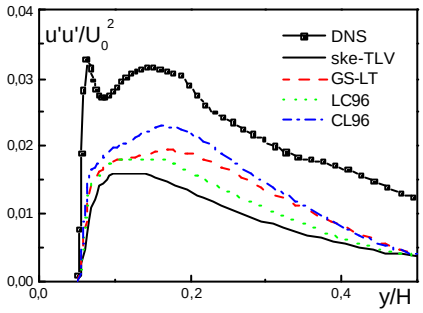


( c ) Normalized turbulent intensity

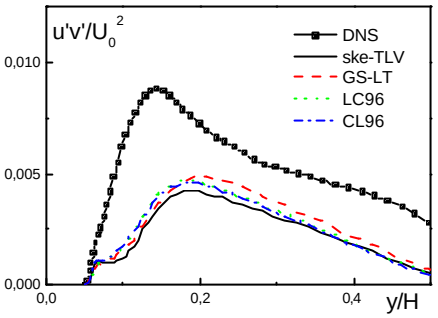


(d) Normalized Reynolds shear stress

Figure 6: Comparison with Maas & Schumann's [2] DNS computation at x/H=1.0

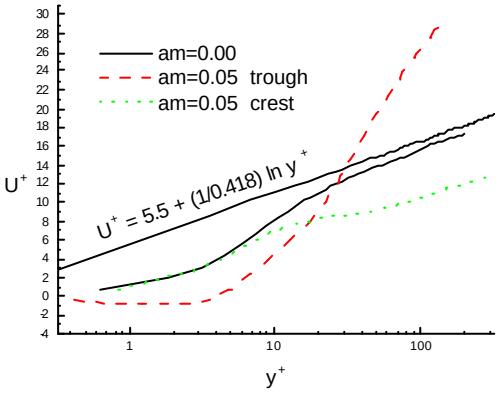


(a) velocity profile

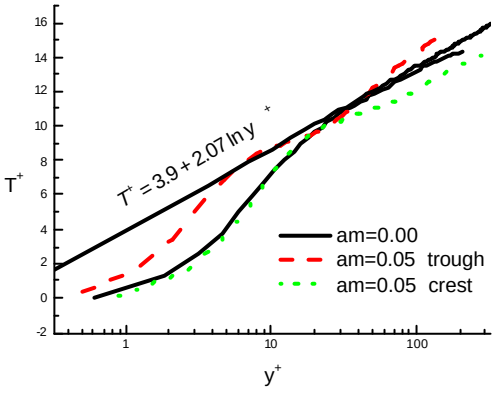


(b) temperature profile

Figure 7: Law of wall for Velocity and temperature at trough and crest of the wavy wall, am=0.05.

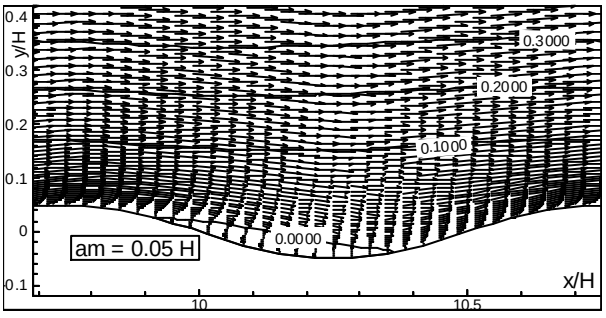


Figure 8: Stream function and vector plot for amplitude wave 0.05 H.

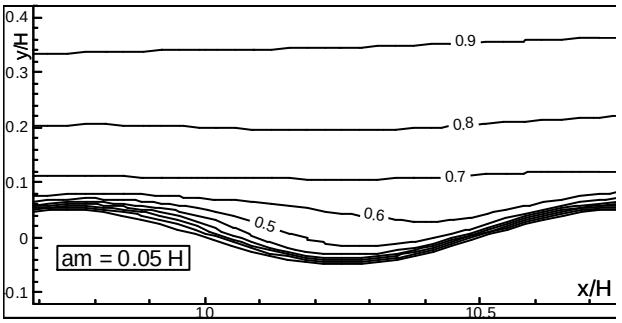


Figure 9: Contours of a dimensional temperature for amplitude wave of 0.05 H.